Research Square

Preprints are preliminary reports that have not undergone peer review.
They should not be considered conclusive, used to inform clinical practice,
or referenced by the media as validated information.

AB-2004, an autism candidate therapeutic, drives distinct taxonomic and functional potential changes in the gut microbiome of wild-type and Shank3B-/- mice

Ashley Franks

A.Franks@latrobe.edu.au

Edden Subejano
Anya Shindler
La Trobe University https://orcid.org/0000-0002-1517-9264
Jennifer Wood
Vic Lin
Angela Jimenez Perez
Alexandra Smith
Mitra Mohsenipour
Elisa Hill
RMIT University https://orcid.org/0000-0002-4146-7198

Article

Keywords:

Posted Date: November 23rd, 2026

DOI: https://doi.org/10.21203/rs.3.rs-11669950/v1

License: This work is licensed under a Creative Commons Attribution 4.0 International License.
Read Full License

Additional Declarations: Yes The authors declare that the small molecule therapeutic AB-2004 discussed in this paper was provided by Axial Therapeutics, Inc., which also funds the PhD projects of MaSES, VL, ARJP, and AHS. The funder had no role in the interpretation or discussion of this work. All perspectives and conclusions presented here are solely those of the authors.

AB-2004, an autism candidate therapeutic, drives distinct taxonomic and functional potential changes in the gut microbiome of wild-type and *Shank3B*$^{-/-}$ mice

M[a] S. Edden Subejano[1], Anya E. Shindler[1], Jennifer L. Wood[1], Vic Lin[2], Angela R. Jimenez Perez[2], Alexandra H. Smith[2], Mitra Mohsenipour[2], Elisa L. Hill-Yardin[2,3], Ashley E. Franks[1*]

[1]Department of Microbiology, Anatomy, Physiology and Pharmacology, School of Agriculture, Biomedicine and Environment, La Trobe University, Bundoora, Victoria, Australia

[2]School of Health and Biomedical Sciences, Royal Melbourne Institute of Technology University, Bundoora, Victoria, Australia

[3]Department of Anatomy & Physiology, The University of Melbourne, Parkville, Victoria, Australia

*Corresponding Author:

Professor Ashley E. Franks

Rm 409 R.L. Reid Building, Department of Microbiology, Anatomy,

Physiology & Pharmacology, School of Agriculture, Biomedicine and Environment,

La Trobe University, Plenty Road, Bundoora, VIC 3086, Australia

Email: A.Franks@latrobe.edu.au

RUNNING TITLE: Gut Microbiome Shifts Induced by AB-2004

Word count: Abstract: 240; Main text: 5 048

ABSTRACT

The gut microbiome is increasingly implicated in the pathophysiology of autism spectrum disorder (ASD), with reports of compositional and functional dysbiosis. Microbially derived metabolites, including 4-ethylphenol and *p*-cresol are associated with heightened levels of anxiety and irritability seen in ASD. AB-2004 is an investigational therapeutic designed to sequester these metabolites, but its effects on gut microbial ecology in mice remain uncharacterised. We examined the impact of AB-2004 on the gut microbiome in the *Shank3B*$^{-/-}$ mouse model of autism as well as wild-type (WT) littermate controls. Mouse faecal DNA across nine timepoints underwent 16S rRNA amplicon sequencing, diversity analyses, differential abundance testing, functional-potential inference, and random forest classification. AB-2004 induced distinct taxonomic and functional shifts in both genotypes. Alpha diversity changes were significant only in WT animals, while beta diversity differed between treated and control groups in both genotypes. Differential abundance analysis identified treatment-associated changes in Lachnospiraceae and Muribaculaceae and shifts in KEGG orthologs mapping to microbial communication, cell-wall remodelling, and aminobenzoate degradation, suggesting competitive pathway diversion as a candidate mechanism. Random forest models reliably discriminated treated from control animals and identified candidate microbiome biomarkers of treatment response. Overall, AB-2004 selectively modulates taxonomic and functional profiles without broadly disrupting microbial community structure. These data suggest AB-2004 may influence microbial pathways linked to aromatic compound processing, but mechanisms require direct validation. This study provides a foundation for multiomic investigations to determine whether microbiome shifts translate to altered metabolite profiles and host-relevant outcomes.

INTRODUCTION

Autism spectrum disorder (ASD; autism) is a heterogeneous neurodevelopmental condition defined by persistent deficits in social communication and interaction, alongside restricted, repetitive patterns of behaviour, interests, and activities [1]. Classified under a unified diagnostic framework in the Diagnostic and Statistical Manual of Mental Disorders, Fifth Edition (DSM-5), ASD spans a continuum from minimal to substantial support needs, with some individuals also having intellectual disability and/or limited verbal communication. Core features typically emerge within the first two to three years of life [1–3]. Co-occurring conditions are common, including anxiety disorders in roughly 45.7% and behavioural or conduct problems in nearly 58% of individuals [4].

In 2021, the global age-standardised prevalence of ASD was estimated at 1 in 127 (788.3 per 100 000; 95% UI 663.8–927.2) [5]. In the United States, an estimated 1 in 31 eight-year-olds is diagnosed with ASD [6], up from 1 in 36 in 2020 [7]. In Australia, an estimated 290 900 individuals (1.1% of the population) were diagnosed with autism in 2022, a 41.8% increase from 205 200 individuals (0.8%) in 2018, with 73% having profound or severe limitation [8], while a 2020 study reported a prevalence of 1 in 23 (4.36%) among children aged 12–13 years [9].

The aetiology of ASD is multifactorial, arising from gene–environment interactions in which genetic influences predominate [10,11]. Over 100 genes have been implicated in autism [12], alongside proposed environmental risk factors including diet, maternal infection, toxin exposure, and gut microbiome changes [13,14]. Variants in the ASD-associated *SHANK3* gene (SH3 and multiple ankyrin repeat domains 3) cause Phelan McDermid Syndrome, in which 63% of individuals are also diagnosed with ASD and commonly experience gastrointestinal issues alongside complex behaviours [15].

The Shank3 scaffolding protein is expressed at excitatory synapses and essential for synapse formation, maturation, and maintenance [16]. Mouse models harbouring *SHANK1*, *SHANK2*, or *SHANK3* variants consistently display ASD-relevant traits such as increased repetitive behaviours, impaired social interactions, and anxiety-like behaviour [16–18], with S*HANK3*-deficient models also showing reduced dendritic spine density and maturation and impaired synaptic transmission [16,17]. *Shank3B*$^{-/-}$ mice, generated by targeted deletion of the PDZ domain (exons 13–16, eliminating the SHANK3α and SHANK3β isoforms), are among the most extensively characterised preclinical ASD models, displaying repetitive and heightened anxiety-like behaviour, social interaction deficits, altered vocalisations, and excessive self-injurious grooming that worsens with age, producing visible skin lesions by 3–6 months [17,18].

Evidence from human cohorts and animal models implicates the gut microbiome in ASD pathophysiology. Altered gut microbiome composition and abundance has been reported in ASD compared to typically developing individuals [19–26]. These shifts can encourage overgrowth of opportunistic pathogens, causing gut dysfunction such as constipation and abdominal pain, which in some individuals is associated with worsened maladaptive behaviour [27–30]. A 2022 meta-analysis reported that 48.67% of individuals with ASD have at least one gastrointestinal symptom [31].

In the maternal immune activation mouse model of autism, *Bacteroides fragilis* ameliorated microbiome alterations, gut permeability, and ASD-relevant behavioural abnormalities, supporting a mechanistic link between microbial composition, the serum metabolome, and behaviour. Gut-derived metabolites proposed to play roles in ASD, such as 4-ethylphenyl (4-EP) and indolepyruvate, were significantly elevated, while levels of the structurally similar *p*-cresol (4-methylphenol) were also elevated but did not reach statistical significance [13].

Human-to-mouse faecal microbiota transfer experiments have shown that ASD-derived microbiota can induce social and repetitive-behaviour phenotypes and alter brain molecular signatures in recipient mice, offering experimental evidence for a causal link [32,33]. The microbiome–gut–brain axis interacts via neural, immune, endocrine, and metabolic pathways, within which microbial metabolites and neuroactive compounds such as serotonin, GABA, and short-chain fatty acids modulate host neural and immune signalling to modify neurodevelopment and behaviour [34,35].

Gastrointestinal dysfunction is increasingly recognised as a core co-morbidity in ASD, and preclinical *SHANK3* models provide mechanistic evidence that this extends to intestinal barrier impairment. *Shank3B*$^{-/-}$ mice show increased gastrointestinal permeability alongside altered epithelial morphology, slowed gut transit, and reduced colonic contraction velocity [36]. *SHANK3* knockout mice similarly show a leaky epithelial barrier phenotype**,** with reduced transepithelial electrical resistance, increased paracellular permeability, and greater *Salmonella* invasion [37].

Several microbiota-derived metabolites are implicated in ASD including *p*-cresol, its sulphated conjugate *p*-cresol sulphate (*p*CS), as well as 4-ethylphenol and its sulphated form 4-ethylphenol sulphate (4-EPS), all produced from microbial metabolism of the aromatic amino acids tyrosine and phenylalanine [38]. *p*-cresol is consistently elevated in the urine and faeces of individuals with ASD [21,39–42], an observation correlated with symptom severity [39,43]. Elevated 4-EP/4-EPS in urine, plasma, or faeces have similarly been linked to neurological and behavioural changes in ASD [13,44,45]. These metabolites share a phenolic core, and because loss of *SHANK3* impairs gut permeability, a route exists for their enhanced translocation into systemic circulation, positioning them as candidate mediators of anxiety and irritability in ASD.

Growing evidence implicating gut microbial metabolites in human disease has created opportunities to target microbial enzymes and metabolic activities therapeutically. AB-2004 (also known as AST-120), originally developed for chronic kidney disease (CKD), is an oral, gut-restricted small-molecule sequestrant with high affinity for small aromatic and phenolic compounds. In its original CKD indication, AST-120 was shown to reduce circulating uremic toxins of gut bacterial origin [46]. In ASD, AB-2004 is designed to adsorb gut-derived neuroactive metabolites including simple phenols, 4-EPS, *p*CS, 3-indoxyl sulphate (3IS), and related compounds within the gastrointestinal tract before systemic absorption [44].

In an open-label phase 1b/2a trial in 30 adolescents with ASD and gastrointestinal symptoms, 8 weeks of AB-2004 reduced urine and serum levels of several bacterial metabolites, including 4-EPS and *p*CS, improved core ASD behaviour, anxiety, and irritability, and was well tolerated with no drug-related serious adverse events [44]. Its downstream effects on microbial ecology and metabolic function, however, remain incompletely understood. Here, we characterised the effects of AB-2004 on the gut microbiome of wild-type (WT) and *Shank3B*$^{-/-}$ mice using 16S rRNA amplicon sequencing across multiple timepoints to determine whether AB-2004 exerts broader off-target effects on microbial ecology or selectively modulates functionally relevant taxa and pathways. These outcomes generate testable hypotheses regarding its mechanism of action and support evaluation of AB-2004 as a gut-targeted therapeutic strategy for ASD.

MATERIALS AND METHODS

Animal ethics approval and experimental animals

All procedures were approved by the RMIT University Animal Ethics Committee (AEC 26167) and conducted in accordance with the Australian Code for the Care and Use of Animals for Scientific Purposes.

Shank3B$^{-/-}$ mice (formal strain name B6.129-*Shank3tm2Gfng*/J; Jax code: IMSR_JAX:017688), originally generated by The Jackson Laboratory (Bar Harbor, Maine, USA), were obtained from the Animal Resources Centre (Canning Vale, WA, Australia) to establish a breeding colony at RMIT University (Bundoora, Victoria, Australia), maintained on a C57BL/6 background. Heterozygous × heterozygous (*Shank3B*$^{+/-}$ × *Shank3B*$^{+/-}$) crosses were used to generate wild-type and homozygous *Shank3B*$^{-/-}$ offspring for experimental use. Male wild-type (n = 12) and *Shank3B*$^{-/-}$ (n = 16) littermates from the RMIT breeding colony were used in this study.

Administration of AB-2004

Mice were fed either Walter and Eliza Hall Institute (WEHI) chow (9% fat, Product no. 8720610; Barastoc Stockfeeds, Victoria, Australia) or WEHI chow containing 5% AB-2004 (w/w), and tap water *ad libitum*, from 5–12 weeks of age. Mice of both genotypes receiving the same treatment (standard chow or AB-2004-supplemented chow) were semi-group housed (3–5 per cage) in individually ventilated cages with dividers (Allentown, New Jersey, USA). The animal facility room was maintained at 22 ± 1 °C, 50 ± 5% relative humidity, on a 12-h light/dark cycle (lights on 7 AM). Animals were randomly assigned to one of four groups: WT-Control (n = 6), WT-AB-2004 (n = 6), SHANK3-Control (n = 7), and SHANK3-AB-2004 (n = 9).

Faecal sample collection

Faecal pellets were collected one day before AB-2004 administration at 5 weeks of age and then weekly until Week 12. Mice were individually transferred to sterile plastic containers and allowed to produce faecal pellets with all collections performed at approximately the same time of day. Up to five faecal pellets collected within one hour were transferred to sterile cryoprotectant tubes (Greiner Bio-One, Kremsmunster, Austria), stored on ice, and frozen at −80 °C until processing. In total, 248 samples were obtained for microbiome analysis, along with a blank extraction control processed and sequenced alongside the samples to isolate reagent-level contaminants and any introduced during extraction.

DNA extraction and 16S rRNA gene sequencing

Genomic DNA was extracted from faecal samples using the DNeasy PowerSoil Pro Kit (QIAGEN) per the manufacturer's protocol. The V3–V4 region of the bacterial 16S rRNA gene was amplified with primers 341F (5'-CCTACGGGNGGCWGCAG-3') and 805R (5'-GACTACHVGGGTATCTAATCC-3') using the following cycling conditions: initial denaturation at 98°C for 30 s; 25 cycles of 98°C for 10 s, 55°C for 30 s, and 72°C for 30 s; final extension at 72°C for 2 min. Dual indexing was performed with the Nextera XT Index Kit (Illumina), with PCR run on a CFX Connect thermal cycler (Bio-Rad). Amplicons were purified with AMPure XP beads (Beckman Coulter), quantified with the Qubit dsDNA BR Assay Kit (Invitrogen), and equimolar pooled libraries sequenced paired-end (2 × 300 bp) on an Illumina MiSeq using the MiSeq Reagent Kit v3.

Sequencing processing and quality control

Raw demultiplexed reads were imported into QIIME 2 (v2024.2) [47]. Primer and adapter sequences were removed using the cutadapt [48] plugin. Only forward reads were used, with

reads showing a maximum expected error greater than 2.0 discarded. Denoising was performed with the DADA2 [49] plugin using default parameters, including consensus chimera removal, to generate amplicon sequence variants (ASVs), which formed the basis for all subsequent diversity and taxonomic analyses.

Taxonomic classification

Taxonomic assignment used a Naive Bayes classifier trained on 16S rRNA gene sequences and taxonomy from the Genome Taxonomy Database Release R220 (GTDB-R220; v220.0) [50], with all other parameters at QIIME 2 defaults (confidence threshold 0.7), yielding a .qza artifact for downstream analyses.

Alpha diversity and statistical analyses

Sequencing depth was normalised in RStudio (2024.9.1.394) [51] by rarefying each sample to 10 500 reads using phyloseq (v1.28.0) [52]; samples below this threshold (n = 29) were excluded to maintain equal sampling effort. Alpha diversity was quantified using the Shannon index, Chao1 richness, and Simpson's evenness. Normality of residuals was assessed with the Shapiro–Wilk test and equality of variances with Levene's test (both $\alpha = 0.05$). Metrics satisfying both assumptions were analysed by one-way ANOVA, with Tukey's HSD post-hoc test applied to significant results ($p < 0.05$) to identify differing group pairs. Analyses used the stats (v4.4.1) [53] and car (v3.1.3) [54] packages; boxplots with individual data points were generated using ggplot2 (v3.5.2) [55].

Beta diversity and statistical analyses

Unrarefied ASV counts were normalised to relative abundances by total-sum scaling (TSS), and a Bray–Curtis dissimilarity matrix was calculated on the TSS-normalised table. NMDS produced a two-dimensional ordination preserving rank-order relationships while minimising

stress, with points coloured by group and 95% confidence ellipses overlaid. Pairwise PERMANOVA was conducted on the Bray–Curtis distances using pairwiseAdonis (v0.4.1) [56] with 999 permutations and Benjamini–Hochberg correction, evaluating Genotype, Treatment, and Timepoint main effects and their two- and three-way interactions. Homogeneity of multivariate dispersion was also assessed for the same factors, with distances to group centroids compared via one-way ANOVA to confirm equivalent within-group variance before interpreting PERMANOVA results.

Relative abundance analysis

Relative-abundance analyses were conducted on TSS-normalised data, dividing each taxon's raw count by its sample's total read count. Taxa with cumulative relative abundance <0.3% across all samples were removed to reduce sequencing noise and spurious low-abundance features [57]; this filtering may exclude rare taxa of potential biological relevance, so results were interpreted accordingly. The remaining dataset was collapsed at the phylum, class, family, and genus levels via microbiome (v1.28.0) [58], and visualised as stacked barplots stratified by experimental group.

Functional prediction via PICRUSt2

Functional metagenome prediction from 16S rRNA gene amplicon data was performed using the full PICRUSt2 pipeline (v2.6.0) with the PICRUSt2-SC (Sugar-Coated) reference database [59], via the single-script workflow (picrust2_pipeline.py), executing the four core steps detailed in the PICRUSt2 full-pipeline-script and producing both stratified and unstratified KEGG Ortholog (KO) and Enzyme Commission gene-family abundance tables. Only the KO tables were used for downstream functional analysis.

Taxonomic and functional differential abundance analysis

Taxonomic and functional differential abundance were assessed using MaAsLin2 (v1.18.0) [60] under a common modelling framework. For taxonomic analysis, ASV counts were transposed to a sample × ASV matrix and centred log-ratio (CLR)-transformed; for functional analysis, an unstratified PICRUSt2 pathway abundance matrix and sample metadata were used to construct a feature table (features × samples), with missing values set to zero, duplicate feature-sample entries summed, and the resulting matrix CLR-transformed. In both cases, sample metadata were converted to a data frame with experimental factors encoded as ordered factors with reference levels Genotype: WT, SHANK3; Treatment: Control, AB-2004; Timepoint: T0–T8.

The fixed-effects model comprised the three main factors (Genotype, Treatment, Timepoint), all pairwise interactions, and the three-way interaction, with Animal ID and Cage Number as random effects and WT/Control/T0 as the reference baseline throughout. Features with FDR $q < 0.05$ were retained. Significant taxonomic features were annotated by effect type and visualised at the genus level as a horizontal bar chart ordered by estimated coefficient, while significant functional features were annotated by coefficient source and exported as a final table of significant KOs for downstream analysis.

Random Forest Modelling using Taxonomic Features and PICRUSt2-predicted KEGG Orthologs (KOs)

Given the high dimensionality of microbiome data relative to sample size, model outputs were interpreted with caution, and emphasis was placed on cross-validation performance and permutation testing rather than individual feature importance alone. A random forest classifier was trained on CLR-transformed ASV relative abundances (prevalence threshold ≥ 2%) and CLR-transformed predicted metagenome pathway abundances (prevalence threshold >= 20%)

using permutation-based variable importance (ranger). Model performance was evaluated using leave-one-animal-out (LOSO) cross-validation (28 folds), with each fold withholding all 9 timepoints from one animal. Preprocessing (prevalence filtering, CLR transformation, near-zero variance removal) was applied within each LOSO fold to prevent data leakage. Statistical significance was assessed by a subject-level permutation test (n = 1000) in which Treatment labels were shuffled at the animal level to preserve within-animal temporal correlations; *p*-values were computed with the +1 correction of Phipson & Smyth [61].

RESULTS

Similar patterns or compositions of microbial communities at the phylum and class levels

Relative abundance analysis aggregated to the phylum (Figure 1A) and class (Figure 1B) levels showed that treatment with AB-2004 did not produce a high-level, wholesale change in the gut microbiome composition of either WT or *Shank3B*$^{-/-}$ mice. All groups were dominated by the phyla Bacteroidota (formerly Bacteroidetes), Bacillota (formerly Firmicutes), and Actinomycetota (formerly Actinobacteria), and by the classes Bacteroidia, Erysipelotrichia, Clostridia, Bacilli, and Coriobacteriia, with only minimal AB-2004-associated changes in Erysipelotrichia and Bacilli.

Treatment alters family and genus level microbial community in WT and Shank3B$^{-/-}$ *mice*

At the family level (Figure 1C), all groups were dominated by the same taxa, with notable AB-2004-associated expansions of Lactobacillaceae and Staphylococcaceae in both WT and *Shank3B*$^{-/-}$ mice; Staphylococcaceae was absent in the untreated WT control group. At the

genus level (Figure 1D), AB-2004-treated groups showed moderate depletion of unclassified Muribaculaceae and *Dubosiella* (more pronounced in *Shank3B*$^{-/-}$), expansion of *Ligilactobacillus*, and moderate depletion of unclassified Lachnospiraceae, alongside expansions of *Enterocloster*, *Ileibacterium*, and *Staphylococcus*.

AB-2004 impacts gut microbial diversity, richness, and evenness in WT mice

Alpha diversity analysis revealed a pronounced effect of AB-2004 on the wild-type group. Shannon diversity was significantly lower in WT-AB than WT-CONT (Figure 2A); WT-CONT showed the highest Shannon diversity of all groups, suggesting a more even distribution across mid-abundant taxa; the remaining groups showed comparable profiles.

Species richness was likewise greater in WT-CONT than WT-AB (Figure 2B), indicating AB-2004 reduced the total number of species in the wild-type gut microbiome. Notably, we observed that SHANK3-CONT samples showed greater richness than WT-AB. Within the *Shank3B*$^{-/-}$ group, AB-2004 did not significantly affect species richness, suggesting the rare biosphere was selectively altered in wild-type but not *Shank3B*$^{-/-}$ mice.

WT-CONT samples showed higher Simpson's evenness than all other groups (Figure 2C), indicating a more uniform distribution of dominant taxa. AB-2004 treatment thus shifted relative dominance structure in the WT group. Simpson's evenness did not differ between SHANK3-CONT and SHANK3-AB (Figure 2C), indicating AB-2004 did not alter dominant taxa distribution in the *Shank3B*$^{-/-}$ group. Analyses at pre- (T0), mid- (T4), and post-treatment (T8) timepoints showed no significant group differences (data not shown), indicating no consistent time-driven pattern.

AB-2004 drives microbial communities to look less similar

Bray-Curtis dissimilarity visualised by NMDS (stress = 0.19) revealed significant compositional differences in gut microbial communities, with AB-2004-treated animals exhibiting greater within-group dissimilarity than controls (Figure 3). Genotype-stratified NMDS plots further showed clear separation between treatment and control animals within both the WT (Supplementary Figure 1) and *Shank3B*$^{-/-}$ genotypes (Supplementary Figure 2). PERMANOVA revealed significant main effects of genotype ($R^2 = 0.031$, $p = 0.001$) and treatment ($R^2 = 0.062$, $p = 0.001$) and a significant genotype × treatment interaction ($R^2 = 0.028$, $p = 0.001$). Timepoint and all timepoint-involving interactions were non-significant (all $p \geq 0.945$), indicating no time-driven compositional shift (data not shown). Pairwise comparisons confirmed significant differences between all group pairs (all p.adjusted = 0.001). PERMDISP also detected significant differences in within-group dispersion ($p = 0.014$), with AB-2004-treated groups showing greater mean distance to centroid (SHANK3-AB2004 = 0.474, WT-AB2004 = 0.459) than controls (SHANK3-CONT = 0.413, WT-CONT = 0.367). Given this dispersion difference, results indicate treatment-associated differences in community structure, though the relative contribution of centroid shifts versus variance cannot be fully disentangled and should be interpreted cautiously.

AB-2004 drives selective community remodelling

Differential abundance analysis using MaAsLin2 identified several ASVs significantly associated with AB-2004 treatment (Figure 4A). Within Muribaculaceae, treatment was associated with enrichment of *Duncaniella muricolitica* and *Duncaniella muris* but depletion of *Paramuribaculum intestinale*, unclassified *Paramuribaculum*, and *Duncaniella dubosii*, suggesting species-level specificity in the response within this family. Within Lachnospiraceae, treatment was predominantly associated with depletion, including unclassified

Lachnospiraceae MD308 and UBA3282, with only a small number of unclassified ASVs enriched. Additional depleted taxa included *Dubosiella newyorkensis* (Erysipelotrichaceae), *Desulfovibrio* sp. (Desulfovibrionaceae), and *Limosilactobacillus* sp. (Lactobacillaceae), while enriched taxa beyond Muribaculaceae included *Adlercreutzia mucosicola* (Eggerthellaceae), *Hominiventricola* sp. (Lachnospiraceae), *Ligilactobacillus* sp. (Lactobacillaceae), and *Ileibacterium valens* (Erysipelotrichaceae). Collectively, these findings suggest AB-2004 drives a compositional shift characterised by enrichment of select Bacteroidota members alongside broad depletion of specific Bacillota, most notably within Lachnospiraceae.

AB-2004 treatment shifts predicted functional capacity

Predicted functional analysis using PICRUSt2 and MaAsLin2 identified several KO features significantly associated with AB-2004 treatment (Figure 4B). Of particular relevance to ASD, AB-2004 treatment was associated with enrichment of 4-hydroxybenzoate decarboxylase subunit C (bsdC; coef = 7.66, $q < 0.05$) within the aminobenzoate degradation pathway, alongside enrichment of KOs involved in cell wall metabolism (ycgQ), amino acid metabolism via Stickland fermentation (grdG), and copper transport (ycnJ). Depleted KOs included those involved in nitrogen metabolism (nasA/nasC), nicotinate and nicotinamide metabolism (pntB), protein repair and quality control (ppm), lipopolysaccharide biosynthesis (wbdD), and cell-cell communication via quorum sensing (rgg2; coef = -6.51). These findings suggest AB-2004 shifts predicted microbial functional capacity across multiple biological processes relevant to host-microbiome interactions in ASD, though direct validation is required.

Random forest pinpoints critical taxa for prediction

A random forest classifier trained on CLR-transformed ASV composition discriminated between AB-2004-treated and control animals with high accuracy under leave-one-animal-out (LOSO) cross-validation, with a pooled LOSO AUC of 0.971 (95% CI: 0.952–0.990)

(Supplementary Figure 3), confirmed as statistically significant by subject-level permutation testing ($p = 0.001$, n = 1 000 permutations). Of 8 241 input ASVs, a median of 734 features per fold were retained after prevalence filtering and near-zero variance removal. The top-ranked features by permutation-based variable importance were an unclassified *Lepagella* sp. (mean VIMP = 0.062 ± 0.032), two unclassified Lachnospiraceae ASVs (0.035 ± 0.010 and 0.025 ± 0.006), an unclassified *Prevotella* sp. (0.022 ± 0.013), and an unclassified Eggerthellaceae sp. (0.022 ± 0.012) (Figure 5A).

Random forest pinpoints critical KOs for prediction

Consistent with the taxonomic classifier, predicted metagenome functional capacity also discriminated between AB-2004-treated and control animals with good accuracy: a random forest classifier trained on CLR-transformed KO abundances achieved a pooled LOSO AUC of 0.916 (95% CI: 0.883–0.949) (Supplementary Figure 4), significant by subject-level permutation testing ($p = 0.001$, n = 1 000 permutations). The five functional features contributing most to class discrimination were class I lanthipeptide synthase (two-component system; quorum sensing) (mean VIMP = 0.010 ± 0.002), LysR family transcriptional regulator, repressor for citA (transcription factor) (0.009 ± 0.002), an uncharacterised protein (0.009 ± 0.002), kappa-carrageenase (glycosidases) (0.004 ± 0.002), and tellurite resistance protein TerA (signalling proteins) (0.003 ± 0.001) (Figure 5B). While these models demonstrate strong discriminatory capacity, they do not imply causal relationships between specific taxa or functions and treatment effects and should be interpreted as identifying candidate features associated with treatment status.

Candidate biomarkers with predictive value and potential functional relevance

To identify taxa with both predictive value and functional relevance, ASVs from the differential abundance analysis were compared with the top 20 VIMP-ranked ASVs from the

random forest classifier; overlapping taxa were prioritised as candidate biomarkers of AB-2004 treatment response (Figure 6). Six taxa were identified in both analyses: *Dubosiella newyorkensis* (Erysipelotrichaceae), *Ileibacterium valens* (Erysipelotrichaceae), unclassified Muribaculaceae UBA7173, unclassified Muribaculaceae, unclassified Lachnospiraceae, and unclassified Lachnospiraceae MD308, spanning two phyla (Bacillota and Bacteroidota). This convergence suggests these taxa are robust candidates for further investigation as microbial biomarkers of AB-2004 treatment response.

DISCUSSION

This study demonstrates that AB-2004 is associated with selective, taxon- and function-level changes in the gut microbiome without large-scale disruption of community structure, conceptually consistent with the emerging paradigm of precision microbiome therapeutics, in which an intervention alters specific metabolic nodes rather than broadly reshaping community composition [62].

The most informative taxonomic signal emerged at family and genus resolution, consistent with the broader observation that ecologically relevant microbial variation is often poorly captured at coarser phylogenetic levels—a principle reflected in microbiome–metabolome studies, where finer taxonomic assignment is generally recommended because coarse bins obscure biologically meaningful variation [63]. Muribaculaceae, Lachnospiraceae, and Erysipelotrichaceae dominated all groups, yet treatment-associated reductions in specific genera, including *Dubosiella* (Erysipelotrichaceae) and unclassified Lachnospiraceae members, were evident. The reduction of *Dubosiella* in the *SHANK3B* cohort is of particular interest given reported role in restoring mucosal barrier function, immunomodulation, and SCFA production [64], though whether its depletion is a direct consequence of AB-2004's

adsorptive action or an indirect effect mediated through substrate competition remains to be established.

Alpha-diversity metrics revealed a genotype-dependent response. WT mice treated with AB-2004 showed reduced richness, evenness, and overall diversity relative to WT controls, whereas *Shank3B*-deficient animals showed no comparable change, possibly reflecting the dysbiotic baseline associated with *Shank3* deficiency [65,66], with these compositional and functional alterations potentially conferring resilience to, or altered sensitivity toward AB-2004-driven perturbations [67,68]. No time-dependent changes were observed in alpha or beta diversity across Timepoints 0, 4, and 8, indicating no progressive community reorganisation within the sampling window. NMDS ordinations of Bray–Curtis distances showed partially overlapping group clusters that were nevertheless significantly distinct by pairwise tests and PERMANOVA, consistent with a treatment-associated compositional shift distinguishable from controls but lacking a strong temporal trajectory. Beta dispersion analysis indicated greater within-group dispersion in AB-2004-treated groups, consistent with increased inter-individual heterogeneity or divergent reassembly trajectories; because unequal dispersion can influence centroid-based significance, the PERMANOVA results should be interpreted with caution. Ecologically, these observations are consistent with loss or suppression of stabilising taxa [69] and with priority effects, where initial community composition and colonisation order predetermine subsequent assembly trajectories [70]. Accordingly, a dysbiotic *Shank3B* baseline may have pre-empted niches, disrupted key interactions, or established alternative networks that buffer against further compositional loss. By contrast, the naive WT community retains unstable niches and stabilising taxa whose suppression drives the observed declines in richness and evenness.

Differential abundance analysis at the genus level showed a phylogenetically heterogeneous response to AB-2004. We observed divergence among closely related taxa within the same family, evidenced by opposing enrichment and depletion patterns among Lachnospiraceae ASVs, and within Muribaculaceae, where consistent enrichment of *Duncaniella* contrasted with depletion of other family members. This argues against broad, lineage-wide competitive exclusion and instead supports metabolic or ecological trait-based selection [71–73] of microbes in response to AB-2004 treatment. Comparable responses have been described for dietary interventions in a gnotobiotic mouse model that enriched specific carbohydrate-active enzymes [74], and in a healthy human cohort under restricted animal-product consumption, where cholesterol biosynthesis and purine degradation pathways were downregulated alongside upregulation of vitamin B2 and tryptophan biosynthesis [75]. These findings underscore the importance of resolving microbial community responses at the ASV level rather than relying on higher-order taxonomic aggregation.

PICRUSt2 analysis revealed a limited number of differentially abundant KOs, with enrichment of aminobenzoate degradation pathways and depletion of cell–cell communication functions. Notably, 4-hydroxybenzoate decarboxylase (4-HBA-DC), which catalyses conversion of 4-hydroxybenzoate (4-HBA) to phenol which is a key step in aromatic compound catabolism, was consistently enriched under AB-2004 treatment [76–78]. Given that AB-2004 is known to sequester phenolic metabolites such as 4-ethylphenol and *p*-cresol in the gut lumen [44], these data suggest that AB-2004 reshapes the luminal aromatic substrate pool, driving compensatory shifts in microbial aromatic amino acid metabolism. We hypothesise that removing downstream phenolics increases flux through alternative tyrosine- and phenylalanine-derived pathways, leading to accumulation of intermediates such as 4-HBA and selective upregulation of enzymes involved in their turnover, including 4-HBA-DC [79–81]. This response likely reflects functional adaptation of the mucosal microbiome to an altered substrate and redox

landscape [82], rather than wholesale taxonomic change. During sustained exposure, such metabolic re-routing may favour taxa encoding anaerobic aromatic processing pathways, contributing to longer-term community restructuring and reducing the availability of phenolic compounds that exert deleterious effects on gut barrier function [83] and neurobiological function [38,84,85].

Although the depletion of several Lachnospiraceae and Muribaculaceae taxa may appear detrimental given that both families are well-established contributors to intestinal butyrate production (beneficial for colonocytes and mucosal barrier function), the selective nature of these depletions may indicate otherwise. It is well documented that Lachnospiraceae, including *Coprococcus*, *Eubacterium*, *Anaerostipes*, and *Roseburia*, are among the principal gut butyrate producers [86,87], while Muribaculaceae produce short-chain fatty acids from dietary polysaccharides and mucin glycans that are positively associated with barrier integrity and reduced inflammation [88]. However, the simultaneous enrichment of functionally competent members within the same families, including *Duncaniella* within Muribaculaceae and some Lachnospiraceae ASVs, suggests trait-based ecological selection favouring taxa adapted to the shifted aromatic substrate landscape, rather than extensive loss of butyrate-producing capacity. The uniform depletion of Lachnospiraceae MD308 alongside enrichment of other family members further argues against broad, lineage-wide competitive exclusion. Instead, these changes appear to reflect fine-grained metabolic niche restructuring driven by AB-2004's action on luminal redox and substrate conditions, consistent with trait-based selection rather than broad functional loss.

The differential abundance analysis of inferred functional capacities broadly supports the hypothesis that AB-2004 remodels the gut microbiome's functional landscape by redirecting aromatic substrate flux. Co-enrichment of an amino acid metabolism KO suggests active processing of the aromatic amino acid pool newly made available by AB-2004, while

enrichment of copper utilisation and cell wall metabolism is consistent with anaerobic taxa undergoing structural and enzymatic adaptation to a shifted redox environment, as copper-dependent enzymes are frequently implicated in aromatic oxidation reactions in anaerobes [89,90]. Conversely, the depletion of quorum sensing and LPS biosynthesis KOs suggests reduced abundance or activity of Gram-negative taxa [91,92], while depletion of nitrogen metabolism and protein repair pathways likely reflects reduced generalised metabolic stress, consistent with a community less taxed by toxic phenolic load [93,94].

The taxonomic and functional random forest analyses highlight features that robustly discriminate treatment groups, providing a prioritised set of candidate taxa and functions for validation. The dominance of Lachnospiraceae and Muribaculaceae among the top VIMP-ranked ASVs is unlikely incidental, as both occupy ecological niches directly relevant to the proposed mechanism of AB-2004 action. Lachnospiraceae are well-characterised producers of butyrate and acetate from saccharolytic fermentation but also encode the aromatic amino acid pathways generating *p*-cresol and phenol [95]. These features place Lachnospiraceae at the metabolic intersection AB-2004 is hypothesised to disrupt. Muribaculaceae, similarly, including the highest-ranked discriminatory ASV, *Lepagella* sp., are key producers of short-chain fatty acids from dietary polysaccharides and mucin glycans, with expansion associated with improved barrier integrity and alleviation of inflammation [88]. The highest-ranked discriminatory function, class I lanthipeptide synthase, is linked to quorum sensing and points to disruption of inter-bacterial communication networks, consistent with the quorum-sensing depletion seen in the differential abundance analysis. Additionally, shifts in cell wall remodelling and cofactor biosynthesis suggest AB-2004 triggers broader reorganisation of microbial functional capacity rather than merely sequestering toxic metabolites passively, favouring taxa encoding the enzymatic machinery to process the rerouted aromatic substrate pool. These findings suggest AB-2004 influences microbial functional organisation beyond

simple luminal adsorption, with favourable implications for gut barrier integrity and homeostatic gut–brain axis function.

Several limitations of this study merit acknowledgement. 16S rRNA amplicon sequencing provides taxonomic resolution and phylogenetic inference but cannot directly assign functions to specific organisms or quantify metabolic fluxes. Consequently, functional predictions generated by PICRUSt2 carry inherent uncertainty, particularly for communities containing poorly characterised or novel taxa, and cannot provide reliable strain-level functional profiling [96]. Because PICRUSt2 infers functional potential from phylogeny rather than direct gene expression measurement, the present data cannot unambiguously distinguish whether observed functional shifts arise from compositional turnover or from within-taxon metabolic reprogramming, in which resident organisms alter gene expression in response to shifting substrate availability without a substantial change in relative abundance. PICRUSt2 results should be interpreted as complementary, hypothesis-generating evidence rather than mechanistic conclusions. In summary, resolving the relative contributions of these processes will require integrating metatranscriptomics and targeted metabolomics in future work.

CONCLUSION

AB-2004 produces a community level reconfiguration of microbiome functional potential that converges, across differential-abundance and machine-learning approaches, on changes in cell wall biology, cofactor and energy metabolism, and xenobiotic processing. This reconfiguration is selective and consistent with shifts in predicted functional potential that may relate to altered substrate availability, although the underlying mechanisms remain to be validated. These findings support the potential of AB-2004 as a targeted microbiome-modulating therapeutic in neurodevelopmental conditions while underscoring the need for multiomic validation to fully characterise its mechanism of action. Future studies integrating metabolomics,

metatranscriptomics, and behavioural phenotyping will be required to determine whether these microbiome changes translate into functional and host-relevant outcomes.

ACKNOWLEDGMENTS

The authors would like to acknowledge funding provided by Axial Therapeutics, Inc. and Dr Stewart Campbell through the Axial-La Trobe Industry HDR Scholarship Agreement.

CONFLICT OF INTEREST

The authors declare that the small-molecule therapeutic AB-2004 discussed in this paper was provided by Axial Therapeutics, Inc., which also funds the PhD projects of M[a]SES, VL, ARJP, and AHS. The funder had no role in the interpretation or discussion of this work. All perspectives and conclusions presented here are solely those of the authors.

REFERENCES

1 American Psychiatric Association. *Diagnostic and Statistical Manual of Mental Disorders*. Fifth. American Psychiatric Association: Washington, DC, USA, 2013.

2 Chawarska K, Klin A, Paul R, Volkmar F. Autism spectrum disorder in the second year: stability and change in syndrome expression. *J Child Psychol Psychiatry* 2007; **48**: 128–138.

3 Webb SJ, Jones EJH. Early Identification of Autism: Early Characteristics, Onset of Symptoms, and Diagnostic Stability. *Infants Young Child* 2009; **22**: 100–118.

4 Salehi M, Jaka S, Lotfi A, Ahmad A, Saeidi M, Gunturu S. Prevalence, Socio-Demographic Characteristics, and Co-Morbidities of Autism Spectrum Disorder in US Children: Insights from the 2020–2021 National Survey of Children's Health. *Children* 2025; **12**. doi:10.3390/children12030297.

5 Santomauro DF, Erskine HE, Mantilla Herrera AM, Miller PA, Shadid J, Hagins H *et al.* The global epidemiology and health burden of the autism spectrum: findings from the Global Burden of Disease Study 2021. *The Lancet Psychiatry* 2025; **12**: 111–121.

6 Shaw K, Williams S, Patrick M. Prevalence and Early Identification of Autism Spectrum Disorder Among Children Aged 4 and 8 Years — Autism and Developmental Disabilities Monitoring Network, 16 Sites, United States, 2022. *MMWR Surveillance Summaries* 2025; **74**: 1–22.

7 Maenner MJ, Warren Z, Williams AR, Amoakohene E, Bakian AV, Bilder DA *et al.* Prevalence and Characteristics of Autism Spectrum Disorder Among Children Aged 8 Years — Autism and Developmental Disabilities Monitoring Network, 11 Sites, United States, 2020. *MMWR Surveillance Summaries* 2023; **72**: 1–14.

8 Australian Bureau of Statistics. Autism in Australia, 2022. ABS, 2024https://www.abs.gov.au/articles/autism-australia-2022.

9 May T, Brignell A, Williams K. Autism Spectrum Disorder Prevalence in Children Aged 12–13 Years From the Longitudinal Study of Australian Children. *Autism Research* 2020; **13**: 821–827.

10 Nakanishi M, Anderson MP, Takumi T. Recent genetic and functional insights in autism spectrum disorder. *Current opinion in neurology* 2019; **32**: 627–634.

11 Taylor MJ, Rosenqvist MA, Larsson H, Gillberg C, D'Onofrio BM, Lichtenstein P *et al.* Etiology of Autism Spectrum Disorders and Autistic Traits Over Time. *JAMA Psychiatry* 2020; **77**: 936–943.

12 Satterstrom FK, Kosmicki JA, Wang J, Breen MS, De Rubeis S, An J-Y *et al.* Large-Scale Exome Sequencing Study Implicates Both Developmental and Functional Changes in the Neurobiology of Autism. *Cell* 2020; **180**: 568-584.e23.

13 Hsiao EY, McBride SW, Hsien S, Sharon G, Hyde ER, McCue T *et al.* Microbiota Modulate Behavioral and Physiological Abnormalities Associated with Neurodevelopmental Disorders. *Cell* 2013; **155**: 1451–1463.

14 Modabbernia A, Velthorst E, Reichenberg A. Environmental risk factors for autism: an evidence-based review of systematic reviews and meta-analyses. *Molecular Autism* 2017; **8**: 13.

15 Levy T, Foss-Feig JH, Betancur C, Siper PM, Trelles-Thorne M del P, Halpern D *et al.* Strong evidence for genotype–phenotype correlations in Phelan-McDermid syndrome: results from the developmental synaptopathies consortium. *Human Molecular Genetics* 2022; **31**: 625–637.

16 Monteiro P, Feng G. SHANK proteins: roles at the synapse and in autism spectrum disorder. *Nature Reviews Neuroscience* 2017; **18**: 147–157.

17 Lin V, Matta SM, Dallman JE, Hosie S, Moreau M, Franks AE *et al.* A Frank Assessment of SHANK: Impacts of Pathogenic Variations in SHANK3 on Preclinical Models of Phelan McDermid Syndrome. *Autism Res* 2025; **18**: 1935–1964.

18 Peça J, Feliciano C, Ting JT, Wang W, Wells MF, Venkatraman TN *et al.* Shank3 mutant mice display autistic-like behaviours and striatal dysfunction. *Nature* 2011; **472**: 437–442.

19 Coretti L, Paparo L, Riccio MP, Amato F, Cuomo M, Natale A *et al.* Gut Microbiota Features in Young Children With Autism Spectrum Disorders. *Frontiers in Microbiology* 2018; **9**: 3146.

20 Dan Z, Mao X, Liu Q, Guo M, Zhuang Y, Liu Z *et al.* Altered gut microbial profile is associated with abnormal metabolism activity of Autism Spectrum Disorder. *Gut Microbes* 2020; **11**: 1246–1267.

21 De Angelis M, Piccolo M, Vannini L, Siragusa S, De Giacomo A, Serrazzanetti DI *et al.* Fecal Microbiota and Metabolome of Children with Autism and Pervasive Developmental Disorder Not Otherwise Specified. *PLoS ONE* 2013; **8**: e76993.

22 Finegold SM, Dowd SE, Gontcharova V, Liu C, Henley KE, Wolcott RD *et al.* Pyrosequencing study of fecal microflora of autistic and control children. *Anaerobe* 2010; **16**: 444–453.

23 Ha S, Oh D, Lee S, Park J, Ahn J, Choi S *et al.* Altered Gut Microbiota in Korean Children with Autism Spectrum Disorders. *Nutrients* 2021; **13**: 3300.

24 Parracho HMRT, Bingham MO, Gibson GR, McCartney AL. Differences between the gut microflora of children with autistic spectrum disorders and that of healthy children. *Journal of Medical Microbiology* 2005; **54**: 987–991.

25 Strati F, Cavalieri D, Albanese D, De Felice C, Donati C, Hayek J *et al.* New evidences on the altered gut microbiota in autism spectrum disorders. *Microbiome* 2017; **5**. doi:10.1186/s40168-017-0242-1.

606 26 Zurita MF, Cárdenas PA, Sandoval ME, Peña MC, Fornasini M, Flores N *et al.* Analysis
607 of gut microbiome, nutrition and immune status in autism spectrum disorder: a case-control
608 study in Ecuador. *Gut Microbes* 2020; **11**: 453–464.

609 27 Chaidez V, Hansen RL, Hertz-Picciotto I. Gastrointestinal Problems in Children with
610 Autism, Developmental Delays or Typical Development. *Journal of Autism and*
611 *Developmental Disorders* 2014; **44**: 1117–1127.

612 28 Dominick KC, Davis NO, Lainhart J, Tager-Flusberg H, Folstein S. Atypical behaviors in
613 children with autism and children with a history of language impairment. *Research in*
614 *Developmental Disabilities* 2007; **28**: 145–162.

615 29 Ferguson BJ, Marler S, Altstein LL, Lee EB, Akers J, Sohl K *et al.* Psychophysiological
616 Associations with GastrointestinalSymptomatology in Autism Spectrum Disorder. *Autism*
617 *Research* 2017; **10**: 276–288.

618 30 Robb AS. Managing irritability and aggression in autism spectrum disorders in children
619 and adolescents. *Developmental Disabilities Research Reviews* 2010; **16**: 258–264.

620 31 Wang J, Ma B, Wang J, Zhang Z, Chen O. Global prevalence of autism spectrum disorder
621 and its gastrointestinal symptoms: A systematic review and meta-analysis. *Frontiers in*
622 *Psychiatry* 2022; **13**: 963102.

623 32 Sharon G, Cruz NJ, Kang D-W, Gandal MJ, Wang B, Kim Y-M *et al.* Human Gut
624 Microbiota from Autism Spectrum Disorder Promote Behavioral Symptoms in Mice. *Cell*
625 2019; **177**: 1600–1618.

33 Kang D-W, Adams JB, Gregory AC, Borody T, Chittick L, Fasano A *et al.* Microbiota Transfer Therapy alters gut ecosystem and improves gastrointestinal and autism symptoms: an open-label study. *Microbiome* 2017; **5**: 10.

34 Cryan JF, O'Riordan KJ, Cowan CSM, Sandhu KV, Bastiaanssen TFS, Boehme M *et al.* The Microbiota-Gut-Brain Axis. *Physiological Reviews* 2019; **99**: 1877–2013.

35 Mayer EA, Tillisch K, Gupta A. Gut/brain axis and the microbiota. *J Clin Invest* 2015; **125**: 926–938.

36 Eberly GL, Manthey M, Pang KKL, Hussein H, Vargas Paniagua E, Machen S *et al.* Shank3 mutation manifests in abnormal gastrointestinal morphology and function in mice. *Frontiers in Neuroscience* 2025; **19**. doi:10.3389/fnins.2025.1552369.

37 Wei S-C, Yang-Yen H-F, Tsao P-N, Weng M-T, Tung C-C, Yu LCH *et al.* SHANK3 Regulates Intestinal Barrier Function Through Modulating ZO-1 Expression Through the PKCε-dependent Pathway. *Inflammatory Bowel Diseases* 2017; **23**: 1730–1740.

38 Zheng Y, Bek MK, Prince NZ, Peralta Marzal LN, Garssen J, Perez Pardo P *et al.* The Role of Bacterial-Derived Aromatic Amino Acids Metabolites Relevant in Autism Spectrum Disorders: A Comprehensive Review. *Frontiers in Neuroscience* 2021; **15**. doi:10.3389/fnins.2021.738220.

39 Altieri L, Neri C, Sacco R, Curatolo P, Benvenuto A, Muratori F *et al.* Urinary p-cresol is elevated in small children with severe autism spectrum disorder. *Biomarkers* 2011; **16**: 252–260.

646 40 Gabriele S, Sacco R, Cerullo S, Neri C, Urbani A, Tripi G *et al.* Urinary p-cresol is elevated
647 in young French children with autism spectrum disorder: a replication study. *Biomarkers*
648 2014; **19**: 463–470.

649 41 Kang D-W, Ilhan ZE, Isern NG, Hoyt DW, Howsmon DP, Shaffer M *et al.* Differences in
650 fecal microbial metabolites and microbiota of children with autism spectrum disorders.
651 *Anaerobe* 2018; **49**: 121–131.

652 42 Kang D-W, Adams JB, Vargason T, Santiago M, Hahn J, Krajmalnik-Brown R. Distinct
653 Fecal and Plasma Metabolites in Children with Autism Spectrum Disorders and Their
654 Modulation after Microbiota Transfer Therapy. *mSphere* 2020; **5**: e00314-20.

655 43 Persico AM, Napolioni V. Urinary p-cresol in autism spectrum disorder. *Neurotoxicology*
656 *and Teratology* 2013; **36**: 82–90.

657 44 Campbell AS, Needham BD, Meyer CR, Tan J, Conrad M, Preston GM *et al.* Safety and
658 target engagement of an oral small-molecule sequestrant in adolescents with autism
659 spectrum disorder: an open-label phase 1b/2a trial. *Nature Medicine* 2022; **28**: 528–534.

660 45 Needham BD, Adame MD, Serena G, Rose DR, Preston GM, Conrad MC *et al.* Plasma
661 and Fecal Metabolite Profiles in Autism Spectrum Disorder. *Biological Psychiatry* 2021;
662 **89**: 451–462.

663 46 Schulman G, Vanholder R, Niwa T. AST-120 for the management of progression of
664 chronic kidney disease. *Int J Nephrol Renovasc Dis* 2014; **7**: 49–56.

665 47 Bolyen E, Rideout JR, Dillon MR, Bokulich NA, Abnet CC, Al-Ghalith GA *et al.*
666 Reproducible, interactive, scalable and extensible microbiome data science using QIIME
667 2. *Nature Biotechnology* 2019; **37**: 852–857.

48 Martin M. Cutadapt removes adapter sequences from high-throughput sequencing reads. *EMBnet journal* 2011; **17**: 10–12.

49 Callahan BJ, McMurdie PJ, Rosen MJ, Han AW, Johnson AJA, Holmes SP. DADA2: High-resolution sample inference from Illumina amplicon data. *Nature Methods* 2016; **13**: 581–583.

50 Parks DH, Chuvochina M, Rinke C, Mussig AJ, Chaumeil P-A, Hugenholtz P. GTDB: an ongoing census of bacterial and archaeal diversity through a phylogenetically consistent, rank normalized and complete genome-based taxonomy. *Nucleic Acids Research* 2022; **50**: D785–D794.

51 Posit team. RStudio: Integrated Development Environment for R. 2024.http://www.posit.co/.

52 McMurdie P, Holmes S. phyloseq: An R package for reproducible interactive analysis and graphics of microbiome census data. *PLoS ONE* 2013; **8**: e61217.

53 R Core Team. R: A Language and Environment for Statistical Computing. 2024.https://www.R-project.org/.

54 Fox J, Weisberg S. *An R Companion to Applied Regression*. Third edition. Sage: Thousand Oaks, CA, USA, 2019https://www.john-fox.ca/Companion/.

55 Wickham H. *ggplot2: Elegant Graphics for Data Analysis*. Springer-Verlag: New York, USA, 2016.

56 Martinez Arbizu P. pairwiseAdonis: Pairwise Multilevel Comparison using Adonis. 2017.https://github.com/pmartinezarbizu/pairwiseAdonis.

689 57 Reitmeier S, Hitch TCA, Treichel N, Fikas N, Hausmann B, Ramer-Tait AE *et al.* Handling
690 of spurious sequences affects the outcome of high-throughput 16S rRNA gene amplicon
691 profiling. *ISME Communications* 2021; **1**: 31.

692 58 Lahti L, Shetty S. microbiome R package. 2017.http://microbiome.github.io.

693 59 Wright RJ, Langille MGI. PICRUSt2-SC: an update to the reference database used for
694 functional prediction within PICRUSt2. *Bioinformatics* 2025; **41**: btaf269.

695 60 Mallick H, Rahnavard A, McIver LJ, Ma S, Zhang Y, Nguyen LH *et al.* Multivariable
696 association discovery in population-scale meta-omics studies. *PLOS Computational*
697 *Biology* 2021; **17**: e1009442.

698 61 Phipson B, Smyth GK. Permutation P-values should never be zero: calculating exact P-
699 values when permutations are randomly drawn. *Stat Appl Genet Mol Biol* 2010; **9**:
700 Article39.

701 62 Woo AYM, Aguilar Ramos MA, Narayan R, Richards-Corke KC, Wang ML, Sandoval-
702 Espinola WJ *et al.* Targeting the human gut microbiome with small-molecule inhibitors.
703 *Nature Reviews Chemistry* 2023; **7**: 319–339.

704 63 Wakita Y, Shimomura Y, Kitada Y, Yamamoto H, Ohashi Y, Matsumoto M. Taxonomic
705 classification for microbiome analysis, which correlates well with the metabolite milieu of
706 the gut. *BMC Microbiology* 2018; **18**. doi:10.1186/s12866-018-1311-8.

707 64 Zhang Y, Tu S, Ji X, Wu J, Meng J, Gao J *et al.* Dubosiella newyorkensis modulates
708 immune tolerance in colitis via the L-lysine-activated AhR-IDO1-Kyn pathway. *Nature*
709 *Communications* 2024; **15**: 1333.

65 Sauer AK, Bockmann J, Steinestel K, Boeckers TM, Grabrucker AM. Altered Intestinal Morphology and Microbiota Composition in the Autism Spectrum Disorders Associated SHANK3 Mouse Model. *Int J Mol Sci* 2019; **20**. doi:10.3390/ijms20092134.

66 Tabouy L, Getselter D, Ziv O, Karpuj M, Tabouy T, Lukic I *et al.* Dysbiosis of microbiome and probiotic treatment in a genetic model of autism spectrum disorders. *Brain, Behavior, and Immunity* 2018; **73**: 310–319.

67 Sommer F, Anderson JM, Bharti R, Raes J, Rosenstiel P. The resilience of the intestinal microbiota influences health and disease. *Nature Reviews Microbiology* 2017; **15**: 630–638.

68 Fassarella M, Blaak EE, Penders J, Nauta A, Smidt H, Zoetendal EG. Gut microbiome stability and resilience: elucidating the response to perturbations in order to modulate gut health. *Gut* 2021; **70**: 595–605.

69 Banerjee S, Schlaeppi K, van der Heijden MGA. Keystone taxa as drivers of microbiome structure and functioning. *Nature Reviews Microbiology* 2018; **16**: 567–576.

70 Debray R, Herbert RA, Jaffe AL, Crits-Christoph A, Power ME, Koskella B. Priority effects in microbiome assembly. *Nature Reviews Microbiology* 2022; **20**: 109–121.

71 Burke C, Steinberg P, Rusch D, Kjelleberg S, Thomas T. Bacterial community assembly based on functional genes rather than species. *Proceedings of the National Academy of Sciences* 2011; **108**: 14288–14293.

72 Ren Y, Niu J, Huang W, Peng D, Xiao Y, Zhang X *et al.* Comparison of microbial taxonomic and functional shift pattern along contamination gradient. *BMC Microbiology* 2016; **16**: 110.

73 Louca S, Polz MF, Mazel F, Albright MBN, Huber JA, O'Connor MI *et al.* Function and functional redundancy in microbial systems. *Nat Ecol Evol* 2018; **2**: 936–943.

74 Wastyk HC, Fragiadakis GK, Perelman D, Dahan D, Merrill BD, Yu FB *et al.* Gut-microbiota-targeted diets modulate human immune status. *Cell* 2021; **184**: 4137-4153.e14.

75 Emmanouil C, Anezaki M, Simistiras A, Glentis S, Scarmeas N, Hatzis P *et al.* Rapid Remodeling of the Human Gut Microbiome in Response to Short-Term Animal Product Restriction and Associations with Host Molecular Phenotypes. *Advanced Science* 2026; **13**: e15575.

76 Zhang X, Wiegel J. The anaerobic degradation of 3-chloro-4-hydroxybenzoate in freshwater sediment proceeds via either chlorophenol or hydroxybenzoate to phenol and subsequently to benzoate. *Applied and Environmental Microbiology* 1992; **58**: 3580–3585.

77 Zhang X, Wiegel J. Isolation and Partial Characterization of a Clostridium Species Transforming Para-Hydroxybenzoate and 3,4-Dihydroxybenzoate and Producing Phenols as the Final Transformation Products. *Microbial Ecology* 1990; **20**: 103–121.

78 Lupa B, Lyon D, Gibbs MD, Reeves RA, Wiegel J. Distribution of genes encoding the microbial non-oxidative reversible hydroxyarylic acid decarboxylases/phenol carboxylases. *Genomics* 2005; **86**: 342–351.

79 Lenzen C, Wynands B, Otto M, Bolzenius J, Mennicken P, Blank LM *et al.* High-Yield Production of 4-Hydroxybenzoate From Glucose or Glycerol by an Engineered Pseudomonas taiwanensis VLB120. *Front Bioeng Biotechnol* 2019; **7**: 130.

80 Miao L, Li Q, Diao A, Zhang X, Ma Y. Construction of a novel phenol synthetic pathway in Escherichia coli through 4-hydroxybenzoate decarboxylation. *Applied Microbiology and Biotechnology* 2015; **99**: 5163–5173.

81 Li T, Juteau P, Beaudet R, Lépine F, Villemur R, Bisaillon J-G. Purification and characterization of a 4-hydroxybenzoate decarboxylase from an anaerobic coculture. *Can J Microbiol* 2000; **46**: 856–859.

82 Bouranis JA, Tfaily MM. Inside the microbial black box: a redox-centric framework for deciphering microbial metabolism. *Trends in Microbiology* 2024; **32**: 1170–1178.

83 Andriamihaja M, Lan A, Beaumont M, Audebert M, Wong X, Yamada K *et al.* The deleterious metabolic and genotoxic effects of the bacterial metabolite p-cresol on colonic epithelial cells. *Free Radical Biology and Medicine* 2015; **85**: 219–227.

84 Needham BD, Funabashi M, Adame MD, Wang Z, Boktor JC, Haney J *et al.* A gut-derived metabolite alters brain activity and anxiety behaviour in mice. *Nature* 2022; **602**: 647–653.

85 Sandoni L, Asta L, Giompaolo N, Renaldi R, Amaretti A, Rossi M *et al.* The Role of Microbiota Metabolites Propionic Acid, p-Cresol, and 4-Ethylphenyl Sulfate in Autism Susceptibility: A Systematic Review. *Autism Research* 2026; **19**: e70237.

86 Vital M, Pieper Dietmar H., Karch A. Colonic Butyrate-Producing Communities in Humans: an Overview Using Omics Data. *mSystems* 2017; **2**: 10.1128/msystems.00130-17.

87 Singh V, Lee G, Son H, Koh H, Kim ES, Unno T *et al.* Butyrate producers, 'The Sentinel of Gut': Their intestinal significance with and beyond butyrate, and prospective use as microbial therapeutics. *Front Microbiol* 2022; **13**: 1103836.

88 Zhu Y, Chen B, Zhang X, Akbar MT, Wu T, Zhang Y *et al.* Exploration of the Muribaculaceae Family in the Gut Microbiota: Diversity, Metabolism, and Function. *Nutrients* 2024; **16**: 2660.

89 Festa RA, Thiele DJ. Copper: an essential metal in biology. *Curr Biol* 2011; **21**: R877-883.

90 Becam J, Dessertine M, Vergnes A, Aussel L, Ezraty B. Role of the Multicopper Oxidase CueO in Copper Homeostasis Under Anaerobic Conditions in Enterobacteria. *Mol Microbiol* 2025; **124**: 297–309.

91 Papenfort K, Bassler BL. Quorum sensing signal-response systems in Gram-negative bacteria. *Nat Rev Microbiol* 2016; **14**: 576–588.

92 Raina S. Lipopolysaccharides: Regulated Biosynthesis and Structural Diversity. *Int J Mol Sci* 2023; **24**. doi:10.3390/ijms24087498.

93 Sui X, Wang J, Zhao Z, Liu B, Liu M, Liu M *et al.* Phenolic compounds induce ferroptosis-like death by promoting hydroxyl radical generation in the Fenton reaction. *Communications Biology* 2024; **7**: 199.

94 Reissner KJ, Aswad DW. Deamidation and isoaspartate formation in proteins: unwanted alterations or surreptitious signals? *Cell Mol Life Sci* 2003; **60**: 1281–1295.

95 Vacca M, Celano G, Calabrese FM, Portincasa P, Gobbetti M, De Angelis M. The Controversial Role of Human Gut Lachnospiraceae. *Microorganisms* 2020; **8**. doi:10.3390/microorganisms8040573.

96 Douglas GM, Maffei VJ, Zaneveld JR, Yurgel SN, Brown JR, Taylor CM *et al.* PICRUSt2 for prediction of metagenome functions. *Nature Biotechnology* 2020; **38**: 685–688.

795 FIGURE LEGENDS

796 Figure 1. Relative abundance of gut microbial taxa by group at phylum (A), class (B), family
797 (C), and genus (D) levels, comparing AB-2004-treated and control wild-type and *Shank3B*$^{-/-}$
798 animals.

799 Figure 2. Comparison of alpha diversity indices—Shannon (diversity) (A), Chao1 (richness
800 estimator) (B), and Simpson's evenness (evenness) (C)—across experimental groups;
801 AB-2004 significantly impacts diversity, richness, and evenness in wild-type mice; ***<0.001;
802 ** <0.01; *<0.05

803 Figure 3. Beta diversity of gut microbial communities assessed by Bray-Curtis dissimilarity
804 and visualised using non-metric multidimensional scaling (NMDS; stress = 0.19). Each point
805 represents a single sample, coloured by group (red = SHANK3-AB2004; green = SHANK3-
806 CONT; yellow = WT-AB2004; blue = WT-CONT). Ellipses represent 95% confidence
807 intervals.

808 Figure 4. Differential abundance of gut microbial taxonomic composition (A) and inferred
809 functional potential (B) associated with AB-2004 treatment, identified by MaAsLin2. Bars
810 represent features significantly enriched (positive coefficient) or depleted (negative
811 coefficient) in AB-2004-treated animals relative to controls ($q < 0.05$). (A) Taxon-level
812 differential abundance of gut microbial ASVs. (B) Differential abundance of PICRUSt2-
813 predicted KEGG Orthologs (KOs), representing inferred gut microbiome functional potential.

814 Figure 5. Top 20 permutation-based variable importance (VIMP) features from random forest
815 classifiers discriminating AB-2004-treated from control animals, based on gut microbiome
816 taxonomic composition (A) and inferred functional potential (B). Features in both panels are
817 ranked by mean VIMP score aggregated across all 28 leave-one-animal-out (LOSO) cross-
818 validation folds; the x-axis displays the mean permutation importance. (A) Taxonomic features

(based on ASV composition) are annotated to the lowest available taxonomic rank. (B) Inferred functional features (PICRUSt2-predicted KOs) are labelled by their predicted gene product function. *** phosphoenolpyruvate---glycerone phosphotransferase subunit DhaK; dTDP-3,4-didehydro-2,6-dideoxy-alpha-D-glucose 3-reductase; nucleoside deoxyribosyltransferase

Figure 6. Venn diagram comparing ASVs identified by MaAsLin2 differential abundance analysis and the top 20 VIMP-ranked ASVs from the random forest classifier. Overlapping taxa, identified in both analyses, are prioritised as candidate biomarkers of AB-2004 treatment response, representing features with both statistically confirmed differential abundance and predictive discriminatory value. Non-overlapping taxa reflect features unique to each analytical approach.

FIGURES

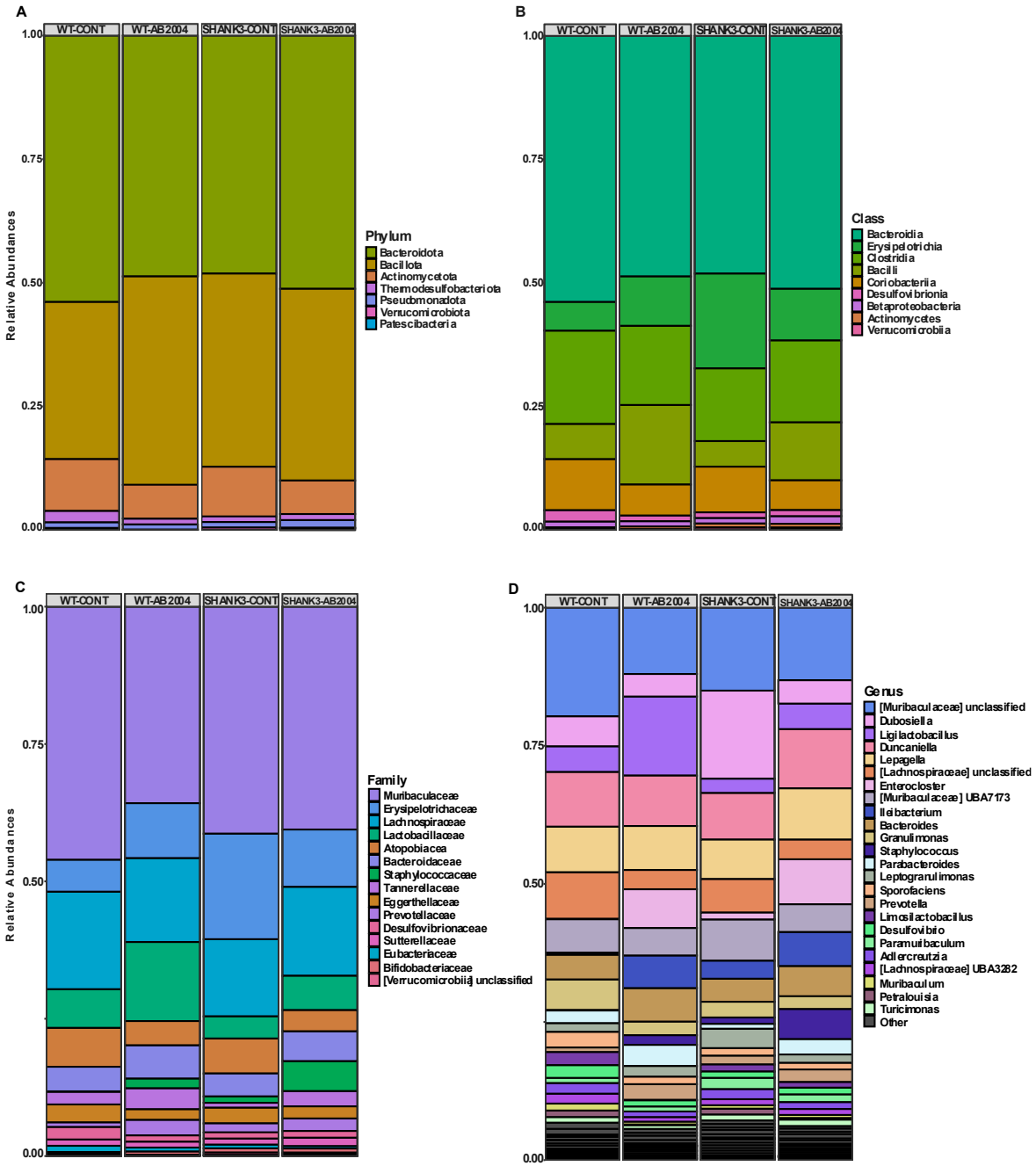


Figure 1. Relative abundance of gut microbial taxa by group at phylum (A), class (B), family (C), and genus (D) levels, comparing AB-2004-treated and control wild-type and *Shank3B*$^{-/-}$ animals.

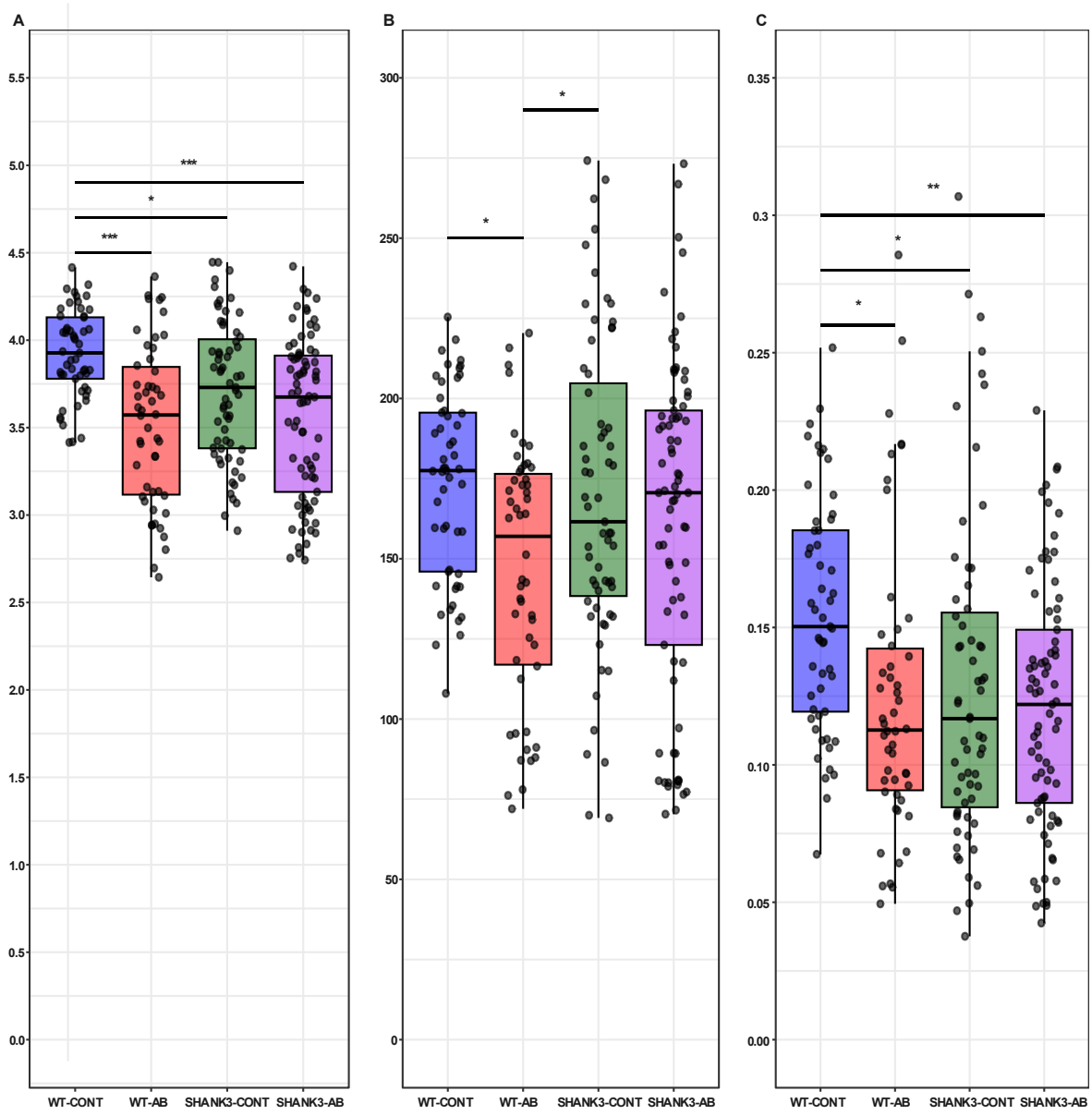


Figure 2. Comparison of alpha diversity indices—Shannon (diversity) (A), Chao1 (richness estimator) (B), and Simpson's evenness (evenness) (C)—across experimental groups; AB-2004 significantly impacts diversity, richness, and evenness in wild-type mice; ***<0.001; **<0.01; *<0.05

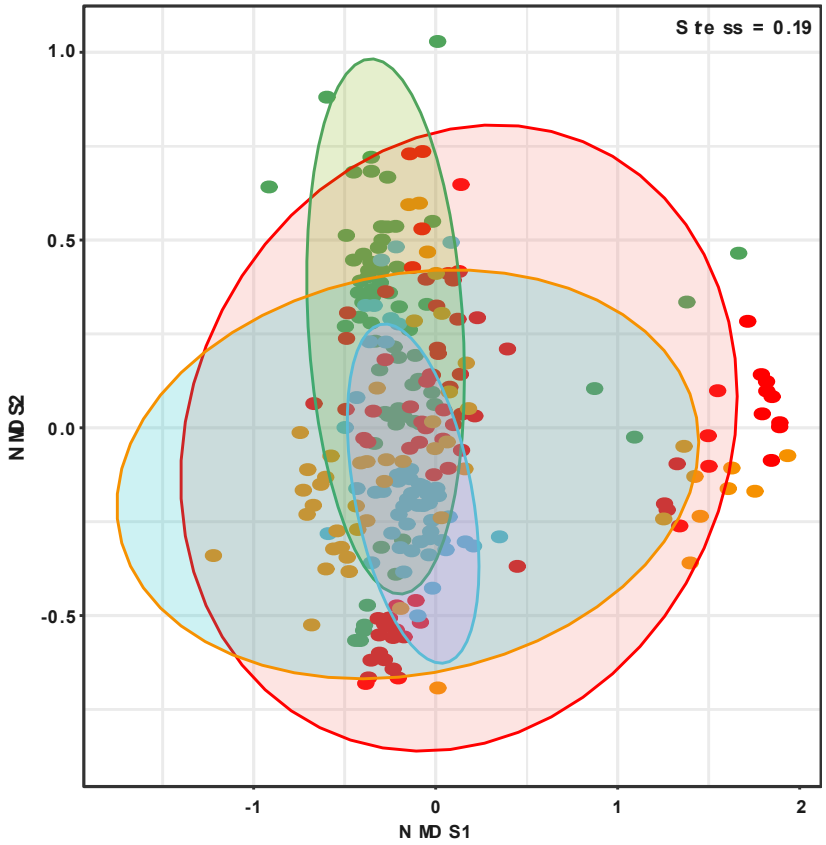
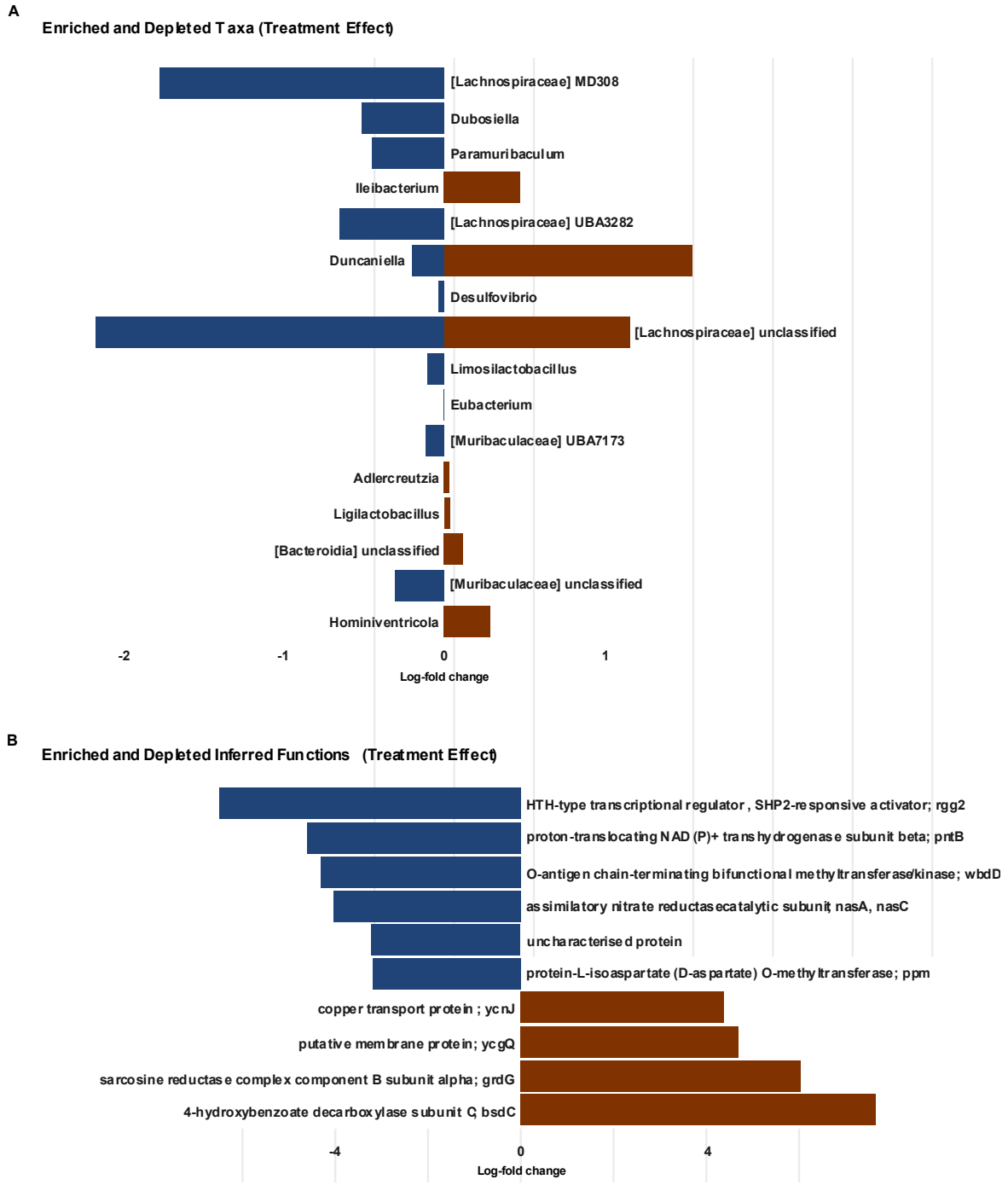


Figure 3. Beta diversity of gut microbial communities assessed by Bray-Curtis dissimilarity and visualised using non-metric multidimensional scaling (NMDS; stress = 0.19). Each point represents a single sample, coloured by group (red = SHANK3-AB2004; green = SHANK3-CONT; yellow = WT-AB2004; blue = WT-CONT). Ellipses represent 95% confidence intervals.



879 Figure 4. Differential abundance of gut microbial taxonomic composition and inferred
880 functional potential associated with AB-2004 treatment, identified by MaAsLin2. Bars
881 represent features significantly enriched (positive coefficient) or depleted (negative
882 coefficient) in AB-2004-treated animals relative to controls ($q < 0.05$). (A) Taxon-level
883 differential abundance of gut microbial ASVs. (B) Differential abundance of PICRUSt2-
884 predicted KEGG Orthologs (KOs), representing inferred gut microbiome functional potential.

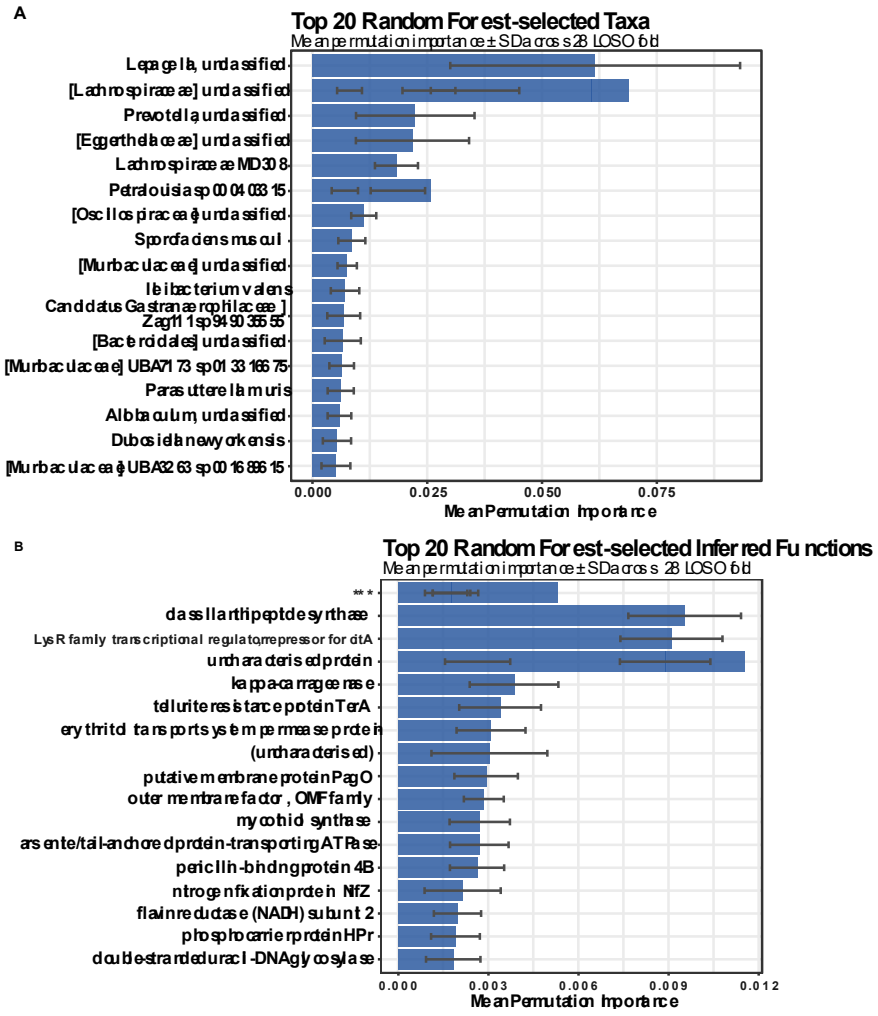
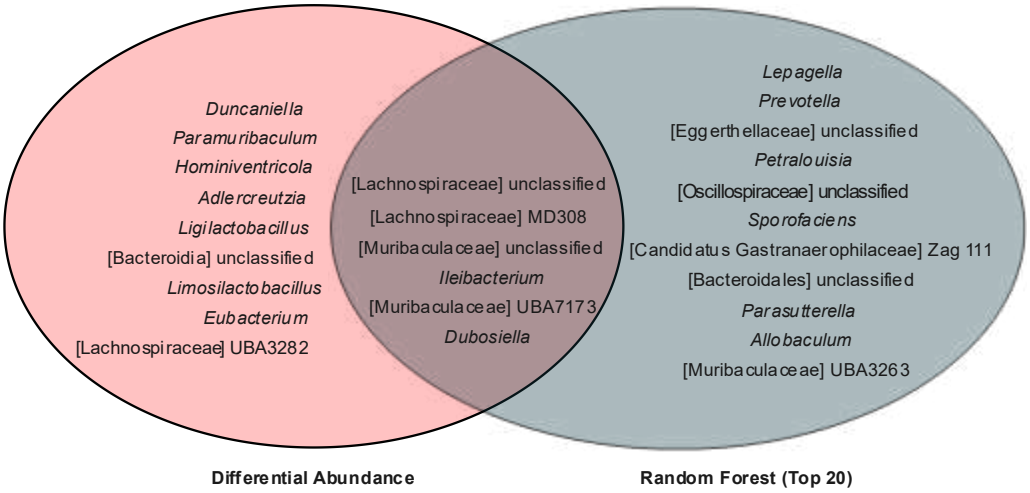


Figure 5. Top 20 permutation-based variable importance (VIMP) features from random forest classifiers discriminating AB-2004-treated from control animals, based on gut microbiome taxonomic composition and inferred functional potential. Features in both panels are ranked by mean VIMP score aggregated across all 28 leave-one-animal-out (LOSO) cross-validation folds; the x-axis displays the mean permutation importance. (A) Taxonomic features (based on ASV composition) are annotated to the lowest available taxonomic rank. (B) Inferred functional features (PICRUSt2-predicted KOs) are labelled by their predicted gene product function. *** phosphoenolpyruvate---glycerone phosphotransferase subunit DhaK; dTDP-3,4-didehydro-2,6-dideoxy-alpha-D-glucose 3-reductase; nucleoside deoxyribosyltransferase



907 Figure 6. Venn diagram comparing ASVs identified by MaAsLin2 differential abundance
908 analysis and the top 20 VIMP-ranked ASVs from the random forest classifier. Overlapping
909 taxa, identified in both analyses, are prioritised as candidate biomarkers of AB-2004 treatment
910 response, representing features with both statistically confirmed differential abundance and
911 predictive discriminatory value. Non-overlapping taxa reflect features unique to each analytical
912 approach.

913

914

Supplementary Files

This is a list of supplementary files associated with this preprint. Click to download.

- SupplementaryFigures.docx